A&A 378, 1078–1086 (2001)
DOI: 10.1051/0004-6361:20011156

Astronomy & Astrophysics

2D-spectroscopy of the Evershed flow in sunspots

J. Hirzberger[1,2] and F. Kneer[1]

[1] Universitäts-Sternwarte, Geismarlandstraße 11, 37083 Göttingen, Germany
[2] Institut für Geophysik, Astrophysik und Meteorologie, Universitätsplatz 5, 8010 Graz, Austria

Received 28 March 2001 / Accepted 16 August 2001

Abstract. The radial variation of the Evershed flow in two small sunspots (NOAA 8737 and NOAA 9145) is studied by means of two-dimensional spectrograms of high spatial resolution. We find a systematic decrease of the flow velocity with photospheric height and a shift of the velocity maximum towards larger penumbral radii in higher layers but no clear correlation between flow velocity and continuum intensity. At the outer penumbral boundaries the Evershed flow ceases abruptly and even downward directed flow velocities in the deepest probed photospheric layers were found. Furthermore, granules adjacent to the penumbral boundary show a systematic redshift of their spot-side parts which is attributed to fast, eventually supersonic, downflows between them and the penumbral boundary.

Key words. Sun: photosphere – sunspots – Sun: granulation – techniques: spectroscopic

1. Introduction

Since its discovery (Evershed 1909) the Evershed effect is a controversial topic in solar physics. It is characterized by a radial outflow in the penumbra of sunspots which abruptly ceases at its outer boundary. This can be concluded from the observed Doppler shifts of spectral lines. But the lines are not only shifted but very asymmetric (see e.g. Bumba 1960; Maltby 1964; Stellmacher & Wiehr 1980). Consequently, the Evershed flow must be highly structured. Indeed several authors (e.g. Beckers 1968; Rimmele 1995a; Shine et al. 1995) have found that the flow is mainly concentrated in the dark penumbral filaments. These findings are contradicted by observations of Wiehr & Stellmacher (1989) and Lites et al. (1990) who did not find a correlation between continuum intensity and flow velocity. Furthermore, observational results of e.g. Stellmacher & Wiehr (1980), Ichimoto (1987) and Balthasar et al. (1997) show an increase of the line asymmetry but a decrease of the line core shifts the higher the lines are formed and even an inversion of the flow direction in the uppermost regions of the photosphere and in the chromosphere (Alissandrakis et al. 1988; Börner & Kneer 1992; Rimmele 1995a). A widely accepted explanation for this result is that the Evershed flow is concentrated in dark almost horizontal flow channels (inclination angle $\phi = 6°-11°$, see Shine et al. 1995) whereas in the bright filaments the matter is at rest. This theory is supported by observations of the penumbral magnetic field structure. Polarimetric measurements of e.g. Beckers & Schröter (1969), Schmidt et al. (1992), Wiehr (2000), and Westendorp Plaza et al. (2001a) show that the magnetic field is divided into two components: (i) field lines which are strongly inclined and located in bright filaments and (ii) almost horizontal field lines which coincide with the dark Evershed channels. A more detailed discussion of observational results and further references can be found in Wiehr (1999).

The origin of the Evershed flow can be explained by the so-called siphon model (Meyer & Schmidt 1968; Thomas 1988; Montesinos & Thomas 1993, 1997). In this model it is assumed that the flows follow magnetic loops and are driven by unbalanced gas pressure due to the stronger magnetic field outside the spot than in the penumbra. Alternative explanations were given by Maltby & Erikson (1967) and Bünte et al. (1993) who proposed that the velocity fields are rather related to acoustic or magneto-acousic waves than to real mass flows.

Numerical simulations of the penumbral regime were performed by Schlichenmaier et al. (1998) who have modelled the penumbral filaments by thin flux tubes which carry the Evershed flow. According to this model the flux tubes are vertical below the photosphere and point radially outward above the photosphere. Indications for fast upward flowing matter in the inner penumbra which would confirm this model view can be seen in observational results from Johannesson (1993) and Rimmele (1995a,b).

At the outer penumbral boundary several observers (e.g. Wiehr & Balthasar 1989; Title et al. 1993; Wiehr & Degenhardt 1994; Balthasar et al. 1996) have found

Send offprint requests to: J. Hirzberger,
e-mail: jhirzbe@uni-sw.gwdg.de

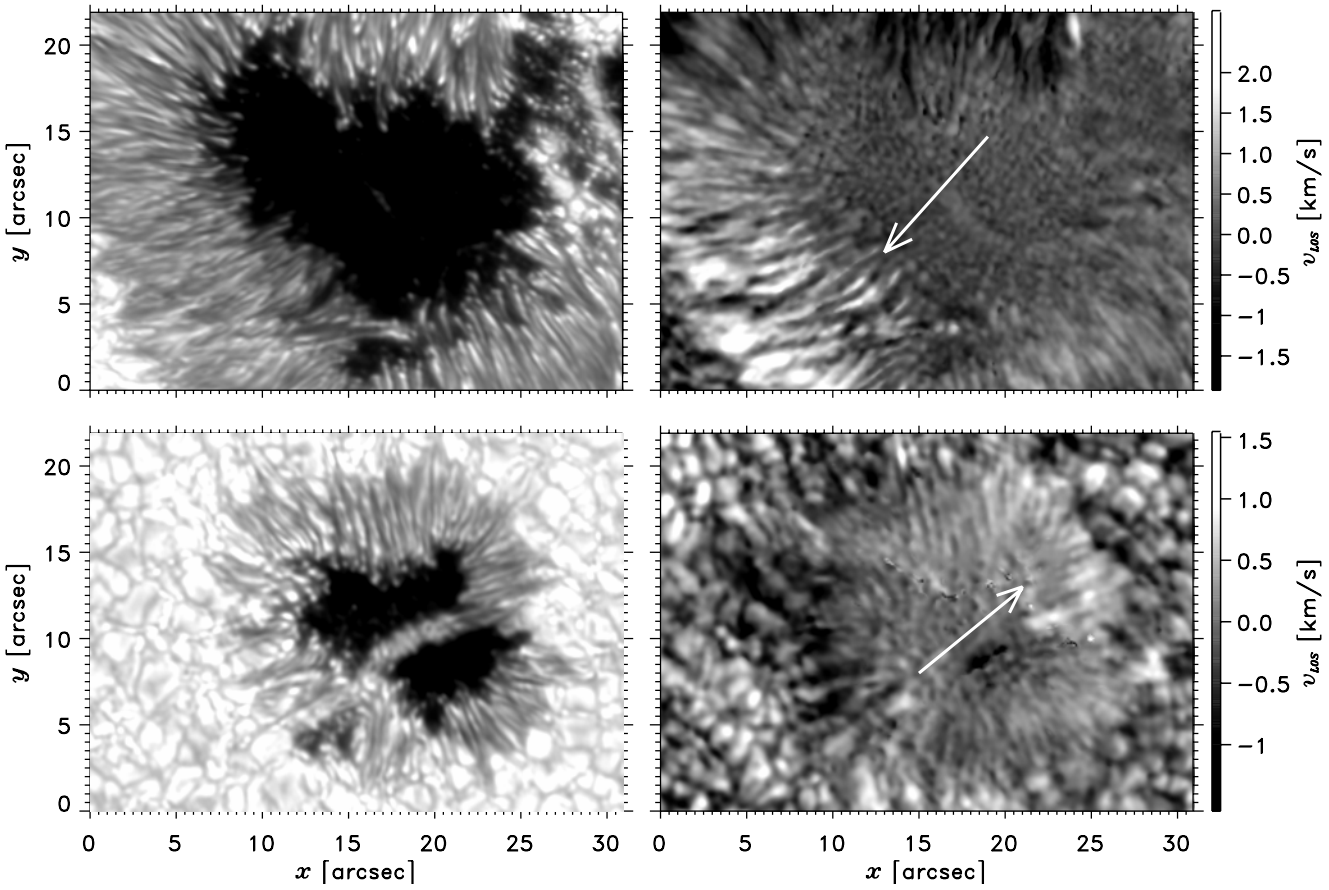

Fig. 1. Broad band images (left panels) and Doppler maps ($i = 50\%$, right panels) of NOAA 8737 at Fe I 5576 Å (upper pannels) and of NOAA 9145 at Fe I 7090 Å (lower panels). Positive velocities (bright regions) represent blueshifts. Arrows indicate the direction to disk center.

an abrupt drop of the flow velocity whereas others (Alissandrakis et al. 1988; Börner & Kneer 1992; Rimmele 1995b) have found a continuation of the flow beyond the outer penumbral boundary. Solanki et al. (1994) have found a sharp drop of the Evershed flow in the low photosphere but a continuation of it in the higher so-called superpenumbral canopy.

To satisfy the continuity equation sinks of the outward transported matter must exist at the endpoints of the flow channels, independently whether the flow ceases just at the penumbral boundary or continues further out. Observational evidence for a subduction of matter below the photosphere were given in Rimmele (1995b) and Westendorp Plaza et al. (1997). Recent observations of Schlichenmaier & Schmidt (2000) and Westendorp Plaza et al. (2001b) show that the inclination of the Evershed flow channels becomes larger than 90° in the outer penumbra which means that the matter turns back below the photosphere in a relatively flat angle. However, an alternative explanation (see Thomas 1981) for an abrupt drop of the flow might be that the flow channels become transparent beyond the penumbra.

In this paper we present results from two-dimensional (2D) sprectroscopic measurements of sunspot penumbrae. We present new insights into the geometry of the Evershed flow from the analysis of high spatial resolution data.

2. Observations and data reduction

The data for the present study have been obtained on October 23, 1999, and on August 31, 2000, with the "Göttingen" Fabry-Perot interferometer (FPI, see Bendlin et al. 1992; Bendlin & Volkmer 1995) in the 70 cm Vacuum Tower Telescope (VTT) at the Observatorio del Teide, Tenerife. The setup is the same as used in Koschinsky et al. (2001) except that we did not use the Stokes V polarimeter.

We have obtained time sequences of narrow band scans across the non-magnetic Fe I 5576 Å and Fe I 7090 Å lines of two sunspots in NOAA 8737 and NOAA 9145 located at off-center positions of $\theta = 31.2°$ and 19.5°, respectively. The observed spot in NOAA 8737 is one of the major components of a large spot group (Zürich classification E, Kanzelhöhe sunspot drawings); the one observed in NOAA 9145 is the main component in a small C group. The Fe I 5576 Å line was scanned at 11 wavelength positions (separated by a distance of $\Delta\lambda = 35.25$ mÅ) and the Fe I 7090 Å line was scanned at 15 positions

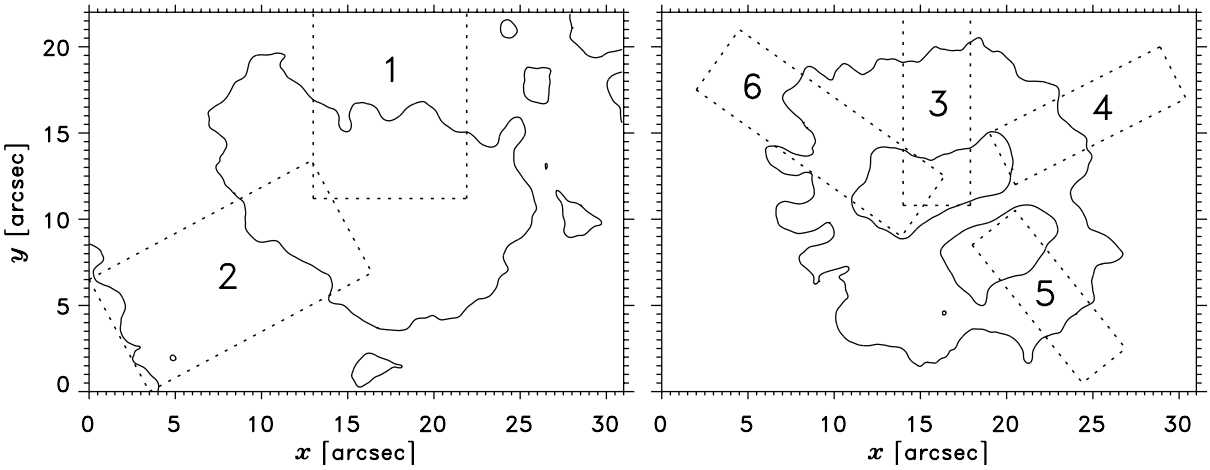

Fig. 2. Location of subfields (dotted boxes) where averaged line-of-sight velocities have been calculated. The solid contour lines mark the inner and outer penumbral boundaries of smoothed images.

($\Delta\lambda = 29.78\,\mathrm{m\AA}$). The effective finesse of the FPI is $\mathcal{F} \approx 30$ and the etalon spacing was set to $d = 1\,\mathrm{mm}$ (Fe I 5576) and to $d = 1.5\,\mathrm{mm}$ (Fe I 7090) so that the bandwidths (*FWHM*) amount to 52 mÅ (Fe I 5576) and 56 mÅ (Fe I 7090), respectively. At each wavelength position 10 images have been recorded. Simultaneously (synchronized by computer control) we have obtained broad band images with filters of 50–100 Å *FWHM* centered at the same wavelengths. The exposure time for all images was set to 20 ms, and the time interval between two scans was 70 s (1999, Fe I 5576 Å) and 47 s (2000, Fe I 7090 Å). The raw images are 384×286 pixel in size and the size of one pixel corresponds to $0\farcs1$.

The data analysis proceeded in essentially the same way as in Hirzberger et al. (2001). Broad band images were reconstructed with speckle interferometric techniques and the reconstruction of the narrow band data was performed by a "quasi"-speckle reconstruction as described in Krieg et al. (1999).

From the reconstructed narrow band scans we can retrieve line profiles at each position in the field of view. Since we expect the spatial resolution of the narrow band data not being better than $0\farcs3$ the line profiles have been averaged by a 3×3 pixel boxcar smoothing. From the bisectors of the resulting line profiles we have computed Doppler shifts (line-of-sight velocities, v_{LOS}) at various intensity levels, $i = (I - I_0)/(I_\mathrm{c} - I_0) \cdot 100$ [%], in the line profile, providing the height variation of v_{LOS} in the photosphere. Here, I_c and I_0 denote the local continuum and line center intensities, respectively, and I is the considered local intensity in the line profile.

Speckle reconstructed broad band images of the two observed sunspots and corresponding Doppler maps from $i = 50\%$ are shown in Fig. 1. The absolute values of the velocities have been calculated by assuming that the umbrae are at rest. The precision of our velocity measurements is in the range of $\Delta v_{\mathrm{rms}} \approx \pm 50\,\mathrm{m\,s^{-1}}$ in the quiet photosphere (cf. Hirzberger et al. 2001) and – due to the lower intensity – about $\Delta v_{\mathrm{rms}} \approx \pm 100\,\mathrm{m\,s^{-1}}$ in the umbra. As can be seen from Fig. 1, the field of view of our optical setup is relatively small which makes it difficult to observe fully developed, mature sunspots. On the other hand, the spatial resolution of our data is significantly enhanced above standard spectroscopic observations due to the application of image reconstruction techniques. It is in the order of $0\farcs3$ for the broad band data and $0\farcs4$–$0\farcs5$ for the narrow band data (Doppler maps).

3. Results and discussion

3.1. Radial variation of the flow

The two observed sunspots shown in Fig. 1 are not exactly radially symmetric. Apart from the appearence of umbral light bridges, especially the penumbrae are severely disturbed. This is the case in the upper right part of NOAA 8737 where instead of a closed penumbra an umbral appendix with many umbral dots is visible and on the lower left side of NOAA 9145 where the penumbra has an almost granular structure instead of radial filaments. We wish to avoid these regions in the present study and scrutinized the Evershed flow in several small subfields where the penumbral filaments are arranged more or less parallel.

The locations of these subboxes are shown in Fig. 2. All of them, except No. 1, include umbral, penumbral, and granular regions. Three of them (2, 3, and 4) cover the center-side part of the penumbrae and subbox No. 1 covers the limb-side penumbra. Subboxes Nos. 5 and 6 cover regions where the line-of-sight is almost perpendicular to the spot radius. The off-center position of NOAA 9145 is with $\theta = 19.5°$ relatively small. Hence, the measured flow velocities are significantly smaller than those in NOAA 8737 (cf. Fig. 1).

In Fig. 3 enlargements of the broad band image and the Doppler map of subfield No. 3 are shown. The high spatial resolution of the data can be seen impressively

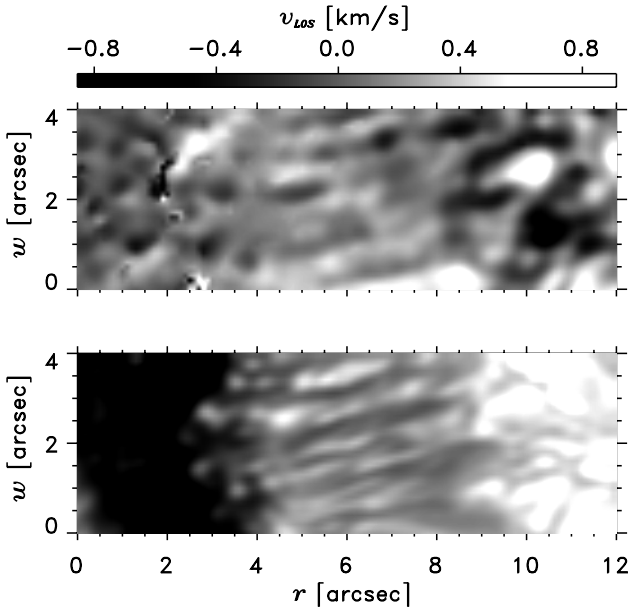

Fig. 3. Broad band intensities (lower panel) and line-of-sight velocities at $i = 50\%$ of subfield No. 3 in NOAA 9145 (cf. Fig. 2).

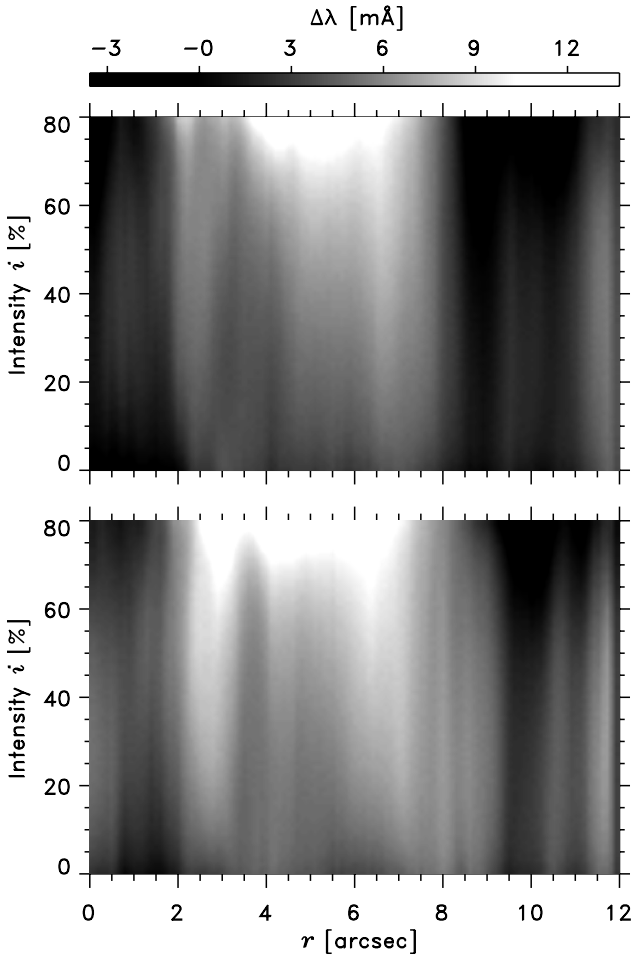

Fig. 4. Averaged bisectorgrams of subfield No. 3. In the upper panel bisectors from line profiles brighter than the local average are shown and in the lower panel bisectors from regions darker than the locally averaged broad band intensitites are displayed. Positive line asymmetries denote blueshifts.

although in the umbra $v_{\rm LOS}$ is somewhat noisy due to the low intensity there. In the penumbral regions a filamentary flow structure can be easily seen also in the velocity field.

In a more quantitative manner Doppler shifts are displayed in Fig. 4. This figure shows line asymmetries depending on the distance from the spot center, r. The line asymmetries are displayed in averaged so-called "bisectorgrams" (see Rimmele 1995a). The bisectors have been computed from averaged line profiles of 22 excellent scans (Fried parameter, $14.8 < r_0 < 15.6$ cm) observed within 27 min. They were further averaged over positions perpendicular to r (co-ordinate w in Fig. 3), but separately according to the brightness in the broad band image. The upper panel of Fig. 4 shows averaged bisectors from those positions along w whose intensity is higher than the average (at r), the lower panel gives the bisectors at positions with intensities lower than the average. With this procedure we are able to separate dark and bright penumbral filaments and granular from intergranular regions outside the spot. The bisectorgrams show an increase of the averaged line-of-sight velocity $\langle v_{\rm LOS}\rangle$ with depth in the photosphere. But the lines are blue-asymmetric in the penumbra and mainly red-asymmetric elsewhere.

In the umbra ($r < 2''$) we measure bisector shifts of ± 5 mÅ and the asymmetries seen in Fig. 4 are mainly resulting from the high noise level in this region. At the inner penumbral boundary ($2'' < r < 3''$) a strong blueshift appears in the darker regions. In the brighter regions a much weaker line asymmetry is visible. The broad band images show several bright "heads" in this region which look similar to comets.

Due to the short off-center position of the sunspot ($\theta = 19.5°$) this result must be interpreted as if we see here footpoints where the Evershed flow comes vertically upward from deeper solar layers. This result agrees well with the findings of Johannesson (1993) and Rimmele (1995a,b) and agrees also with the model simulations of Schlichenmaier et al. (1998). It is remarkable in the present result that this upflows are predominantly visible in regions darker than the mean intensity. Hence, in this boundary region the Evershed flow indeed seems to be concentratred only in the dark channels between the bright "heads". One can see on a movie of the 22 broad band images that these "heads" are moving towards the umbra and some of them are even able to detach from the penumbra and become umbral dots. But obviously these "heads" do not contain the biggest part of the flow.

In the main body of the penumbra ($3\farcs5 < r < 8\farcs5$) we see the "normal" Evershed flow with upward line-of-sight velocities, i.e. outward motion, because the subfield is located in the center-side part of the sunspot. The flow

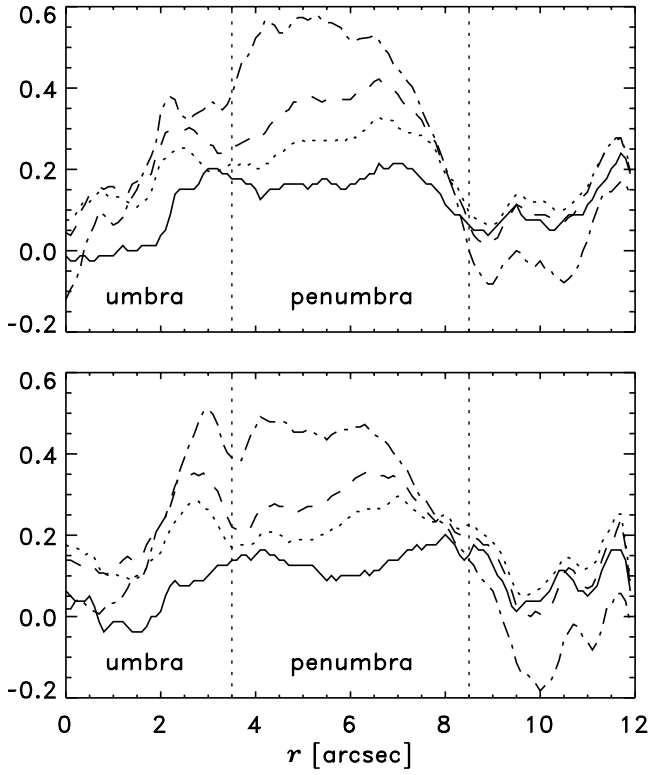

Fig. 5. Line-of-sight velocities extracted from Fig. 4 (subfield No. 3, NOAA 9145) at $i = 0\%$ (solid), $i = 25\%$ (dotted), $i = 50\%$ (dashed), and $i = 75\%$ (dash-dotted). Upper panel: from positions brighter than the local average; lower panel: from positions darker than the average. Vertical dotted lines mark the inner and outer penumbral boundaries (cf. Fig. 3).

is visible in both bright and dark filaments and the velocities are even somewhat higher in the bright filaments than in the dark ones (see Fig. 5 below). The maximum of the flow velocity depends on r and i. The closer the measurements refer to the line core (low i) the more does the maximum velocity shift towards larger r. This means that the Evershed flow is rather inclined than exactly horizontal. It is impossible to estimate the inclination from one singular off-center position of the sunspot, but qualitatively, this result again agrees with the findings of e.g. Rimmele (1995a).

At the outer penumbral boundary ($8\farcs5 < r < 10''$) $\langle v_{\rm LOS}\rangle$ again becomes directed downward. This is seen in both bright and dark regions and is more pronounced close to the continuum than in the line center. Probably we see here the Evershed flow turning back downward into layers beneath the photosphere.

The behaviour of the average line-of-sight velocities $\langle v_{\rm LOS}\rangle$ is depicted in a quantitative manner in Fig. 5 for various i. The measured absolute values of $\langle v_{\rm LOS}\rangle$ are relatively low in the penumbra. This is due to the low θ of the spot's position. The maximum at the inner penumbral boundary and, vice versa, the minimum at the outer penumbral boundary is – as already mentioned – highest in dark regions and close to the continuum, i.e. the observed effects at the penumbral boundaries occur mainly in deep photospheric levels.

In Fig. 6 averaged line-of-sight velocities for subfields Nos. 1–6 are plotted. In this figure bright and dark regions are not discriminated, i.e. the asymmetries were calculated from line profiles averaged over all pixels with constant r. The line profiles from subfields Nos. 1 and 2 (NOAA 8737) have been averaged from 6 consecutive scans with Fried parameter $r_0 > 14.7$ cm and those from boxes Nos. 4–6 from 22 scans as in Figs. 4 and 5. Two common properties of $\langle v_{\rm LOS}\rangle$ can be seen in all subfields: (i) the absolute values of $\langle v_{\rm LOS}\rangle$ are systematically larger close to the continuum than in the line cores and (ii) in all subfields we find a minimum of $\langle v_{\rm LOS}\rangle$ at the outer penumbral boundary, independent whether the subfields are located on the center- or limb-side part of the penumbra. These minima are more pronounced in deeper photospheric layers (continuum level) than in higher ones (line center level).

At the inner penumbral boundary the results are not so clear. We do not find maxima of $\langle v_{\rm LOS}\rangle$ in all of the subfields as seen in subfield Nos. 3. Only in subfields Nos. 1 and 6 small maxima are indicated at $r \approx 4''$ and $r \approx 3''$, respectively. These are the regions of the innermost "cometary heads" which can be found in these two subfields as well. In the fields Nos. 2, 4, and 5 pronounced bright "heads" are not visible. Hence, one might be tempted to relate the "heads" to sources of the Evershed flow although from Figs. 4 and 5 it has to be concluded that the sources or footpoints of the Evershed flow are essentially located in the dark regions between them. Moreover it is remarkable that these upflows at the inner penumbral boundary can only be seen at the limb-side penumbra of NOAA 8737 (Fe I 5576 Å) and at positions of the umbra-penumbra boundary rather perpendicular to the center-limb direction of NOAA 9145 (Fe I 7090 Å) than on the other side. This result might indicate that the visibility of the footpoints is strongly sensitive on the off-center position of the spot and on the formation height of the spectral line. This can also be concluded from the studies of Rimmele (1995a,b).

A particularity in the behaviour of $\langle v_{\rm LOS}\rangle$ appears in subfield No. 2. In the inner penumbra ($4'' < r < 9''$) $\langle v_{\rm LOS}\rangle$ behaves like in all other fields with an increase of the velocity from the line center towards the continuum level and a tendency of the maximum of $\langle v_{\rm LOS}\rangle$ to be shifted outwards in the line center. But at $r = 10''$, $\langle v_{\rm LOS}\rangle$ shows a minimum in all heights. Further outwards the velocities are higher in the line center than close to the continuum. The broad band images exhibit a highly structured penumbra in this subfield (cf. Fig. 1). It looks as if here the bright filaments are ordered in several layers (cf. Maltby 1964). Especially two bright filaments which have their origin at $x = 18''$ and $y = 3''$ seem to cross the entire penumbra. Probably the outer maximum of $\langle v_{\rm LOS}\rangle$ is produced by these two filaments which cross the penumbra in a height where the line center of Fe I 5576 Å is formed.

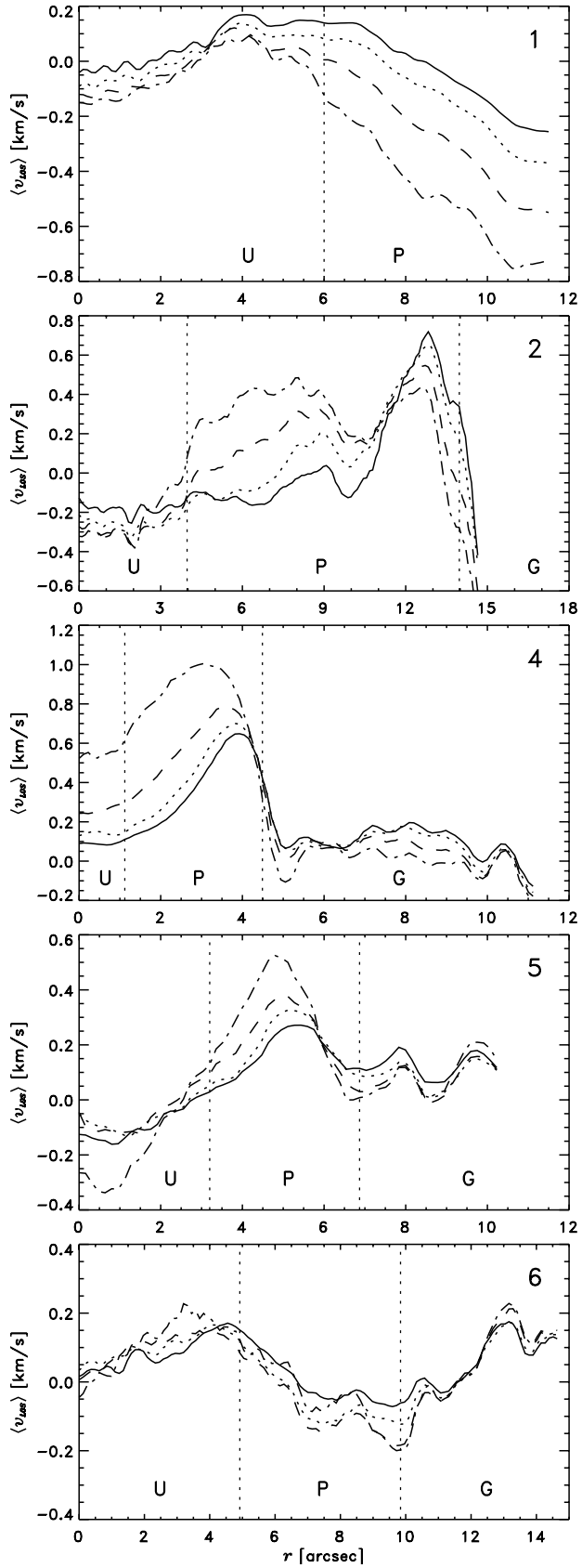

Fig. 6. Mean line-of-sight velocities in subfields Nos. 1, 2, 4, 5, and 6 in dependence on the position, r, along the box. Linestyles are as in Fig. 5. The vertical dotted lines separate umbral (U), penumbral (P), and granular (G) regions.

3.2. Effects at the outer penumbral boundary

In the previous section it has been demonstrated that the mean line-of-sight velocity vanishes at the outer penumbral boundaries confirming earlier findings of several authors (Wiehr & Degenhardt 1994; Balthasar et al. 1996) that the outward directed Evershed flow abruptly ceases there. Furthermore, our results show that just outside the sunspot $\langle v_{\rm LOS}\rangle$ becomes slightly negative, especially in low photospheric heights. These negative $\langle v_{\rm LOS}\rangle$ might be interpreted as downward flows which have been already found by Westendorp Plaza et al. (1997, 2001b) and Schlichenmaier & Schmidt (2000). However, since some penumbral filaments are much longer than others $\langle v_{\rm LOS}\rangle$ contains contributions from different regimes like penumbral, granular, and intergranular regions. Hence, a cancelation of different flow regimes must be considered here.

In Fig. 7 two enlargements of the outer penumbral boundary of NOAA 9145 are displayed. In addition to the broad band images, Doppler maps from $i = 50\%$ overlayed with intensity contours are shown. The contours have been computed using image segmentation techniques based on Fourier filtering of the broad band images (see Hirzberger et al. 1997). As can easily be seen in this figure, those granules which lie next to the penumbral boundary contain a systematically asymmetrical flow field. In the lanes between the penumbra and the granules we detect fast downflows but also the "inner" (spot-side) parts of the granules exhibit redshifts. On a movie of the broad band images these structures show a typical granular evolution. It astonishes that they are granules, in principle, but with velocities systematically distorted by the Evershed flow.

It has to be concluded from our data that this granular asymmetry is not a transitory effect. We find these asymmetric granules all around the spot (and also at the lower left corner of NOAA 8737, cf. Fig. 1) and throughout the entire time series. Moreover, it has been demonstrated by Hirzberger et al. (2001) that our method of determining Doppler velocities leads to an excellent correlation between broad band intensities and flow maps for structures larger than the resolution limit in quiet granulation. In Fig. 8 an enlargement of the granular region around $x = 4''$ and $y = 8''$ (see lower left panel of Fig. 1) is shown. This region does not seem to be affected by the Evershed flow in the sunspot and we find a very good agreement between broad band intensities and Doppler velocities.

A close inspection of the Doppler maps yields that those granules which are located at the endpoints of the Evershed flow channels are significantly disturbed; i.e. they show a redshift in their spot-side parts. A few examples can be found in Fig. 7, but both subfields of Fig. 7 are rather at the center-side than at the limb-side penumbra. The right panels of Fig. 8 show an example of a limb-side penumbra. Here also some aymmetric granules can be detected (e.g. the one close to the center of the subfield). Yet, as already mentioned above, the filamentary structure

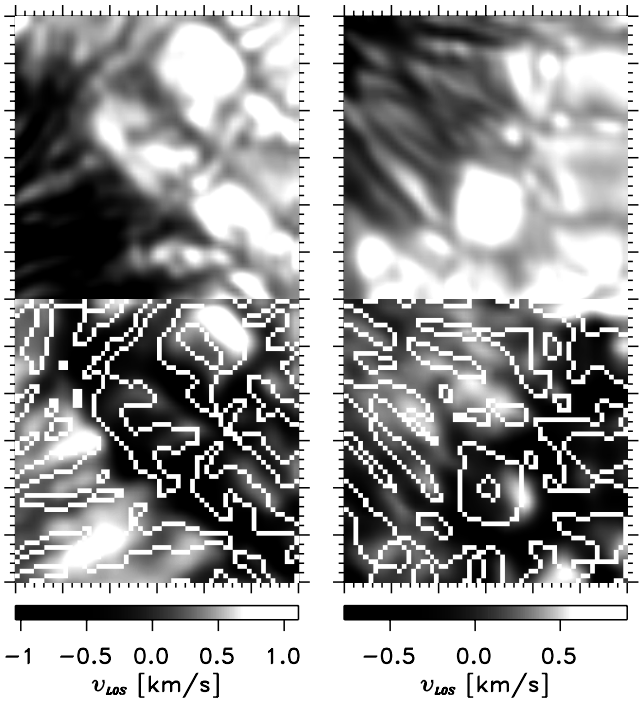

Fig. 7. Two examples for deformed Doppler velocities in granules close to the outer penumbral boundary. In the upper panels broad band images are displayed and in the lower panels Doppler maps (at $i = 50\%$) overlayed with granular contours are shown. Tickmarks are at distances of 0.″2.

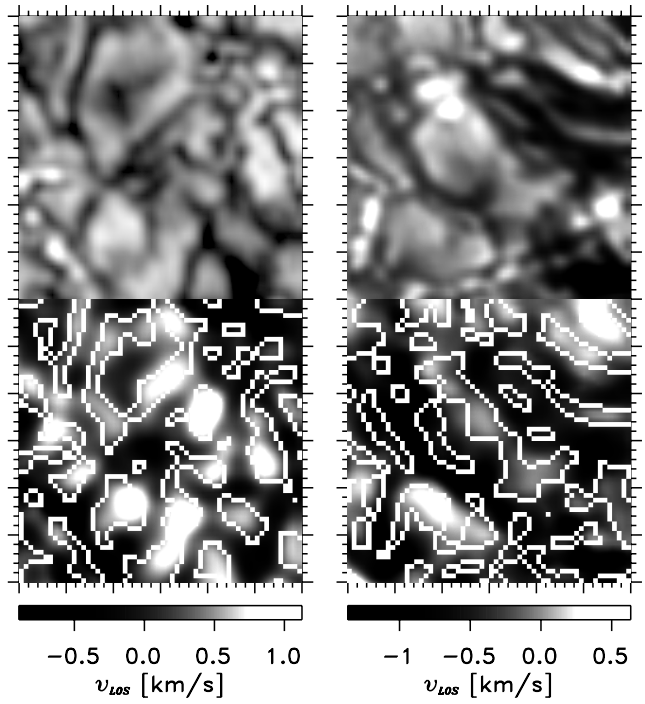

Fig. 8. As Fig. 7 but for a mainly undisturbed granular field (left) and for a subfield at the limb-side penumbra of NOAA 9145 (right).

of the limb-side penumbra of NOAA 9145 is considerably disturbed.

Although the time evolution of the intensity structure of granules close to the outer penumbral boundary is not different from typical quiet granules their internal flow structure seems to be strongly influenced by the Evershed flow. From theoretical models (e.g. Montesinos & Thomas 1993) this result might be explained by the occurence of standing shock fronts when the siphon flows achieve supercritical velocities. Such shock fronts are heated by the dissipation of energy and would appear bright. Yet, this would not explain why bright red-shifted structures behave like quiet granules. This would be – as already proposed by Montesinos & Thomas (1997) – a viable scenario for outward moving bright penumbral grains which are well known from earlier observations (e.g. Schröter 1962; Tönjes & Wöhl 1982; Sobotka et al. 1999) and can also be found in our data.

If we adopt that a strong siphon-effect causes the Evershed flow then fast downflows would be expected at the outer endpoints of the flow channels. According to Montesinos & Thomas (1997) the diameters of the flow channels are typically between 50 km and 70 km at the top at the arch but must be significantly smaller in the low photosphere in order to drive the siphon flow. These sizes are in the range of the mean free path of the photons in the photosphere. Hence, if they are resolvable at all, they are far below the resolution limit of present solar telescopes. Therefore, in observational data the signature of fast downflows between the outer penumbral boundary and adjacent granules, is smeared to much larger structures than their actual size. This might be an explanation why the existence of downflows is not unobjectionably proven so far. A simple – and yet very optimistic – estimation of the average flow velocity $\bar{v}$ in a resolution element with a diameter $D = 290\,\mathrm{km}$ (0.″4) containing one downflow channel with a diameter $d = 50\,\mathrm{km}$ and a velocity of $v = 8\,\mathrm{km\,s^{-1}}$, which is proposed by Montesinos & Thomas (1997) as the maximum speed in a supercritical model above the standing shock front, would give:

$$\bar{v} = \frac{\left(D^2 - d^2\right) u - d^2 v}{D^2} \cos\theta = 0.69\,\mathrm{km\,s^{-1}} \qquad (1)$$

where $u = 1\,\mathrm{km\,s^{-1}}$ is the mean velocity of the granular upflow in the resolution element and $\theta = 19.5°$ as in our data. Consequently, if only one downflow channel is located within the resolution element, the net flow velocity would still be positive. At least four of such channels are needed in one resolution element to yield the observed negative velocities.

4. Summary and conclusions

We have used high resolution 2D spectra to analyze the geometry of the Evershed flows in two sunspots. Our results can be summarized as follows:

1. The flow velocity decreases systematically with photospheric height and the maximum of the flow velocity

shifts towards the outer penumbral boundary in higher photospheric layers. This is in good agreement of former results of e.g. Börner & Kneer (1992) and Rimmele (1995a).

2. At the inner penumbral boundary we find maxima of the line-of-sight velocity in the dark channels between the "heads" of bright penumbral filaments. Upflows at the inner penumbral boundary have been already found in observations of Johannesson (1993) and Rimmele (1995a,b) and agree with model simulations of Schlichenmaier et al. (1998). In regions where we do not see pronounced bright "heads" at the inner boundary, no maxima of $\langle v_{\rm LOS} \rangle$ were found. Probably their appearence in spectroscopic observations is highly dependent on the the off-center position, θ, the formation height of the spectral line, whether the center- or limb-side part of the spot is considered, and on a combination of these parameters.
3. We do not find a general clear correlation between flow velocity and contiuum intensity in the penumbra. Although in several penumbral regions the flow occurs mainly in the darker filaments, in some subfields (cf. Fig. 4) the velocities in the brighter filaments are even higher than in the darker ones. This is in agreement with findings of Wiehr & Stellmacher (1989) and Lites et al. (1990) but in contradiction with results of Beckers (1968), Rimmele (1995a), and Shine et al. (1995) who have found that the Evershed flow appears mainly in the dark penumbral filaments. An explanation for this lack of correlation might be that the spatial resolution of our broad band images is around $0\farcs3$ or even better whereas that of the Doppler images is somewhat lower ($0\farcs4$–$0\farcs5$). It is hence possible that in the broad band images structures appear but cannot be recognized in the Doppler images. However, if the Doppler images are correlated with artificially smoothed broad band images or intensity images computed from the narrow band data (not shown) the results become somewhat less noisy but the correlation is still variable in different penumbral regions.
4. At the outer penumbral boundary we find an abrupt drop of the flow velocities which agrees well with findings of e.g. Wiehr & Balthasar (1989), Title et al. (1993), Wiehr & Degenhardt (1994), and Balthasar et al. (1996). At the center side parts of the penumbrae the line-of-sight velocities become even negative in the deepest probed photospheric layers. This reverse of the flow direction supports the theory of a siphon effect driving the flow. Furthermore, observational evidence for a subduction of matter at the outer penumbral boundary were already given by Westendorp Plaza et al. (1997, 2001b) and Schlichenmaier & Schmidt (2000).
5. The flow fields of granules located next to the outer penumbral boundary is considerably influenced by the Evershed flow; i.e. they exhibit fast downflows in their spot-side parts. According to theoretical models of Montesinos & Thomas (1997) these anormalities might be explained by non-resolved and eventually supersonic downflow channels which are located between the penumbral boundary and adjacent granules.

Acknowledgements. The authors are grateful to an anonymous referee for careful reading and for constructive criticism. Financial support by the Austrian *Fonds zur Förderung der wissenschaftlichen Forschung* (*Erwin-Schrödinger-Stipendium* J1802-PHY and J1976-PHY) is gratefully acknowledged. The Vacuum Tower Telescope is operated by the Kiepenheuer-Institut für Sonnenphysik in Freiburg (Germany) in the Spanish Observatorio del Teide of the Instituto de Astrofísica de Canarias in Tenerife. J.H. thanks the Universitäts-Sternwarte Göttingen for the hospitality and the financial support.

References

Alissandrakis, C. E., Dialetis, D., Mein, P., Schmieder, B., & Simon, G. 1988, A&A, 201, 339
Balthasar, H., Schleicher, H., Bendlin, C., & Volkmer, R. 1996, A&A, 315, 603
Balthasar, H., Schmidt, W., & Wiehr, E. 1997, Solar Phys., 171, 331
Beckers, J. M. 1968, Solar Phys., 3, 258
Beckers, J. M., & Schröter, E. H. 1969, Solar Phys., 10, 383
Bendlin, C., & Volkmer, R. 1995, A&AS, 112, 371
Bendlin, C., Volkmer, R., & Kneer, F. 1992, A&A, 257, 817
Börner, P., & Kneer, F. 1992, A&A, 259, 307
Bumba, V. 1960, Izv. Krim Astr. Obs., 23, 212
Bünte, M., Darconza, G., & Solanki, S. K. 1993, A&A, 274, 478
Evershed, J. 1909, MNRAS, 69, 454
Hirzberger, J., Vázquez, M., Bonet, J. A., Hanslmeier, A., & Sobotka, M. 1997, ApJ, 480, 406
Hirzberger, J., Koschinsky, M., Kneer, F., & Ritter, C. 2001, A&A, 367, 1011
Ichimoto, K. 1987, PASJ, 39, 329
Johannesson, A. 1993, A&A, 273, 633
Koschinsky, M., Kneer, F., & Hirzberger, J. 2001, A&A, 365, 588
Krieg, J., Wunnenberg, M., Kneer, F., Koschinsky, M., & Ritter, C. 1999, A&A, 343, 983
Lites, B. W., Scharmer, G. B., & Skumanich, A. 1990, ApJ, 335, 329
Maltby, P. 1964, Astrophys. Norveg., 8, 205
Maltby, P., & Eriksen, G. 1967, Solar Phys., 2, 249
Meyer, F., & Schmidt, H. U. 1968, Z. Angew. Math. Mech., 4, T218
Montesinos, B., & Thomas, J. H. 1993, ApJ, 402, 314
Montesinos, B., & Thomas, J. H. 1997, Nature, 390, 485
Rimmele, T. 1995a, A&A, 298, 260
Rimmele, T. 1995b, ApJ, 445, 511
Schlichenmaier, R., Jahn, K., & Schmidt, H. U. 1998, A&A, 337, 897
Schlichenmaier, R., & Schmidt, W. 2000, A&A, 358, 1122
Schmidt, W., Hofmann, A., Balthasar, H., Tarbell, T. D., & Frank, Z. A. 1992, A&A, 264, L27
Schröter, E. H. 1962, Z. Astrophys., 56, 183

Shine, R. A., Title, A. M., Tarbell, T. D, Smith, K., & Frank, Z. A. 1995, ApJ, 430, 413
Sobotka, M., Brandt, P. N., & Simon, G. W. 1999, in High resolution solar physics: theory, observations, and techniques, ed. T. R. Rimmele, K. S. Balasubramaniam, & R. R. Radick, ASP Conf. Ser., 183, 116
Solanki, S. K., Montavon, C. A. P., & Livingston, W. 1994, A&A, 283, 221
Stellmacher, G., & Wiehr, E. 1980, A&A, 82, 157
Title, A. M., Frank, Z., Shine, R. A., et al. 1993, ApJ, 403, 780
Thomas, J. H. 1981, in The physics of sunspots, ed. L. E. Cram, & J. H. Thomas, Sunspot NM, Sacromento Peak Obs., 345
Thomas, J. H. 1988, ApJ, 333, 407
Tönjes, K., & Wöhl, H. 1982, Solar Phys., 75, 63
Westendorp Plaza, C., del Toro Iniesta, J. C., Ruiz Cobo, B., et al. 1997, Nature, 389, 47
Westendorp Plaza, C., del Toro Iniesta, J. C., Ruiz Cobo, B., et al. 2001a, ApJ, 547, 1130
Westendorp Plaza, C., del Toro Iniesta, J. C., Ruiz Cobo, B., & Martínez Pillet, V. 2001b, ApJ, 547, 1148
Wiehr, E., & Balthasar, H. 1989, A&A, 208, 303
Wiehr, E., & Stellmacher, G. 1989, A&A, 225, 528
Wiehr, E., & Degenhardt, D. 1994, A&A, 287, 625
Wiehr, E. 1999, in Magnetic Fields and Oscillations, ed. B. Schmieder, A. Hofmann, & J. Staude, ASP Conf. Ser., 184, 86
Wiehr, E. 2000, Solar Phys., 197, 227